Determination of Plasticity following Deformation and Welding of Austenitic Stainless Steel

Acar, MO & Fitzpatrick, ME

Original citation & hyperlink:
Acar, MO & Fitzpatrick, ME 2017, 'Determination of Plasticity following Deformation and Welding of Austenitic Stainless Steel' *Materials Science and Engineering: A*, vol 701, pp. 203-213
https://dx.doi.org/10.1016/j.msea.2017.06.074

DOI 10.1016/j.msea.2017.06.074
ISSN 0921-5093

Publisher: Elsevier

Determination of Plasticity following Deformation and Welding of Austenitic Stainless Steel

M. O. Acar[1,3], M. E. Fitzpatrick[2,3]

[1]Now at: Siemens Energy Inc., Hamilton, New Jersey 08638, USA

[2]Centre for Manufacturing and Materials Engineering, Coventry University, Priory Street, Coventry CV1 5FB, UK

[3] Previously at: Department of Engineering and Innovation, The Open University, Walton Hall, Milton Keynes MK7 6AA, UK

Abstract

Intergranular strain has been associated with high-temperature cracking of welded pipework in 316H austenitic stainless steel material used in nuclear power plant heat exchangers. In this study, neutron diffraction has been used to study the development of intergranular strains in plastically-deformed and welded 316H stainless steel. Measurements have been made of the intergranular strain evolution with increasing plastic strain in base material, and correlated with further measurements made in samples extracted from welded pipes, where the pipes were welded following plastic deformation to different levels of plastic strain. Strong tensile strain evolution was seen on the compliant 200 grain family. The results were

correlated with various proxy measures of plastic strain, including hardness and diffraction peak width, and excellent agreement was obtained.

1. Introduction

In power generation plants, energy is transferred to the power generator turbines *via* heat exchanger units which are exposed to high temperatures and pressures. Many metres of austenitic stainless steel tubes are bent, swaged and welded to produce these heat exchanger units. During tube-shaping and welding operations, plastic deformation takes place. This influences in-service performance of the material unless the effect of plastic deformation is fully annealed out. The ASME Boiler and Pressure Vessel Design code [1] specifies that the limit of forming strain for 316H stainless steel material which is going to operate between 580°C and 675°C is 20%, and if it exceeds that threshold the material should be annealed at a minimum of 1040°C to restore its mechanical properties, tensile strength, creep strength and creep ductility to the start-of-life values. Current construction practices in the UK for 316H tubes forbid welding onto material that has experienced more than 15% plastic strain, without first resolution heat treating the material.

Although the standard codes and construction practices provide some guidance, it is sometimes not possible to follow these rules strictly, especially when the whole boiler is constructed as a large and complex single unit containing different tubing materials. Therefore, tubing material in-service is likely to retain some degree of prior plastic deformation arising from tube-shaping and welding operations.

Plastic deformation is considered as one of the major factors in initiating stress corrosion cracking [2]–[6] and creep failure [7]–[11] of austenitic stainless steels. Creep resistance increases with plastic strain, whereas creep ductility drastically decreases [10].

There is no direct method to accurately determine the degree of plastic deformation to which a material was previously subjected. Hardness measurement and X-ray diffraction peak broadening are used for the qualitative determination of the plastic strain. However, there have been recent promising attempts at the development of experimental methods to measure plastic deformation, based on the observation of crystallographic changes in materials after plastic deformation using neutron diffraction [12], [13] and electron back-scattered diffraction (EBSD) [14].

Elastic anisotropy means that the elastic stiffness of a crystal is dependent on its orientation relative to the applied load. The yield stress may also depend on the orientation of the crystal, which makes the material plastically anisotropic. Because of elastic and plastic anisotropy, austenitic stainless steel has a highly complex stress-strain response [15].

When a material elongates under uniaxial load, the slip direction will tend to rotate towards the loading direction, which means that the grains reorient with increasing plastic deformation. When the load is released, residual strains develop: a combination of residual intergranular strains (Type II) and residual intragranular strains (Type III) [16]. Intergranular strains self-equilibrate over a length scale of the order of the grain size. They develop owing to elastic anisotropy of the grain and the

constraint of neighbouring grains. Intragranular strains are generated over a length scale smaller than the grain size. Their origin is generally crystal defects such as dislocations, solute atoms and vacancies. Hereafter, we focus on the type II intergranular strains and will use the term "residual intergranular strains" as previously used in the literature [17], [18].

Another effect of plastic deformation is the increase in dislocation density and the formation of dislocation bands and arrays. Severe cold working of an annealed metal will increase the dislocation density from around 10^7 to 10^{11} dislocations/cm^2 [19]. In a grain, as the deformation proceeds, dislocations intersect each other and start to lose their mobility, which explains the strain hardening process. With further plastic deformation they begin to condense into bands and arrays. These structures can be considered as low-angle boundaries (LAB) within the grains, where the separation between two crystallographic orientations is only a few degrees, less than in a high-angle grain boundary (>15°) [19].

Diffraction techniques enable tracking of the changes in residual intergranular strains and the dislocation density with increasing plastic deformation. Neutron diffraction is particularly attractive as it has good penetration into metallic alloys (e.g. >50 mm in steel) and is able to measure a defined volume inside a bulk component [20]. The diffraction peak position obtained for an *hkl* plane is shifted depending on the accumulated strain on this plane. The accumulated strain on each plane is different owing to the differences in elastic and plastic anisotropy, and therefore, the peak shift changes for individual planes. By using the peak shifts in a diffractogram, Pang *et al.* measured the residual intergranular strains developed after unloading

from 8% uniaxial straining of a rolled 309H stainless steel in the rolling direction [21]. They constructed residual strain pole figures for the 111, 200, 331 and 224 planes and found that high tensile residual strains develop on the 200 planes in the direction of straining parallel to the rolling direction. Peng *et al.* also measured residual intergranular strains at different specimen orientations in AISI 304 stainless steel with 3 μm grain size after unloading from 7.5, 29.8 and 44.7% uniaxial straining [18]. They observed an almost linear relationship between residual intergranular strains on individual planes in the loading direction and the macroscopic plastic deformation. Intergranular strains measured in samples following plasticity [18], [21], [22] and during *in-situ* tensile testing [23], [24] have shown that intergranular strains which exist following plasticity can be used to provide a semi-quantitative trace of the level of macroscopic plastic deformation that was experienced. Daymond *et al.* [12] proposed an approach to fit the differences in strains observed between the various diffraction peaks to a single parameter called "anisotropy strain". By comparing with calibration data, obtained for example from a uniaxial loading test, a correlation can be drawn between the "anisotropy strain" and the macroscopic plastic strain. This approach has been used for fcc [12], [25] and bcc [26] materials with some success.

Peak widths of individual diffraction peaks are affected by the plastic deformation history of the material, as the strain fields associated with dislocations and vacancies lead to peak broadening [23], [27]: a greater degree of plastic deformation leads to a broader peak.

Electron back scattered diffraction (EBSD) enables the measurement of crystal orientation on a specimen surface. Several researchers have used EBSD measurements, particularly the misorientation angle (the orientation change between adjacent measurement points) distribution in the sampling area to determine the degree of deformation [24], [37]. Das *et al*. combined EBSD with digital image correlation to monitor strain development on slip bands within TRIP steels [38].

In this study, the plastic strain in prestrained and welded tubes was studied using several techniques: neutron diffraction, EBSD, and hardness testing. The measurements provide information on the plastic deformation history in the material after pre-straining and welding. Moreover, the anisotropy strain has been used to quantify the plastic deformation in pre-strained and welded AISI 316H austenitic stainless steel tubes.

2. Experimental Procedure

2.1. Test specimens

A set of five plastically pre-strained and welded tubes were supplied by British Energy (now EDF Energy), UK. The base metal was AISI Type 316H austenitic stainless steel with composition 16.89 wt% Cr, 11.25 wt% Ni, 2.04 wt% Mo, 1.55 wt% Mn, 0.53 wt% Si, 0.089 wt% Co, 0.05 wt% C, less than 0.05% of other elements and the balance being Fe. The grain size of the base material was about 30 μm. The 1% proof strength of the non-strained material was 367 MPa and the Young's modulus for this

material is 195 GPa. The tubing (prior to plastic straining) was approximately 38 mm in (outer) diameter and 4 mm in thickness.

The test specimens were fabricated as follows: (1) four tubes were strained uniaxially in tension up to 10, 15, 20 and 25% total strain in order to simulate plastic deformation associated with fabrication processes in a controlled way. (2) These four strained tubes plus an unstrained tube were cut into two halves. (3) Matching half-tubes were then welded together using a tungsten inert gas (TIG) welding process with Type 316L filler metal.

Samples were extracted from the cross-weld regions and from the ends of the pipes remote from the weld, to study the strained and welded materials separately. Figure 1 shows the locations of samples extracted from the welded tubes.

2.2. Neutron diffraction experiments

2.2.1. Residual intergranular strain and peak width measurements

The ENGIN-X instrument at the UK's ISIS neutron source was used to measure the intergranular strains and peak widths [28]. ENGIN-X has two collimator banks 180˚ apart allowing measurement from two orthogonal scattering vectors at the same time. Lattice strain was measured parallel and perpendicular to the pre-straining direction and at various angles between those directions. ISIS provides a white beam of neutrons to create time-of-flight diffraction patterns. At ENGIN-X the range of the wavelengths available is 0.5-6Å, which means that data are available from a range of

d-spacings. The first four peaks in the diffraction pattern were selected for analysis, namely 111, 200, 220 and 311. To obtain the *d*-spacing and the peak widths of individual peaks a single peak fitting routine implemented in OpenGenie [29] was used. This routine uses a pseudo-Voigt function which fits very well the observed peak profiles in neutron diffraction.

Measurements were performed in the mid-length of the strained specimens to determine intergranular strains and peak width for the various as-strained conditions before welding. Cross-weld specimens with 0 and 20% pre-strain were used to determine the change in intergranular strains and peak width owing to welding by measuring at the weld centre, and at points 7, 9, 12, 16 and 29 mm away from the weld centre line. Since the thickness of the individual strips is small, two nominally-identical strips were glued together in order to improve the counting statistics by using a $3 \times 3 \times 5$ mm^3 gauge volume. Measurements of *d*-spacing at the mid-length of a specimen with no plastic strain were averaged and used as a strain-free reference for each specific *hkl* plane to calculate the residual intergranular strains in the cross-weld and strained specimens.

The peak widths were obtained as full-width at half maximum for each individual diffraction peak. In this paper we present results from the (111) reflection only for conciseness.

2.2.2. Crystallographic texture measurement

Crystallographic textures were determined using the Stress-Spec diffractometer at the FRM-II reactor facility, Germany, using a neutron wavelength of

1.5480 Å. Pole figures for 111 and 200 grain families were obtained by measuring the Bragg peak intensity on a 5° × 5° grid. MTEX software was used for the recalculation of 111, 100, 110 and 311 pole figures from the experimental 111 and 200 pole figures.

2.3. Electron back-scattered diffraction (EBSD)

EBSD measurements were performed using a field-emission scanning electron microscope (Zeiss Supra 55VP FEGSEM) fitted with a Nordlys EBSD detector. EBSD data were obtained by automatically scanning the electron beam with 20 kV accelerating voltage over the polished surface of the specimen which was tilted at 70° from the horizontal. The working distance between the sample and phosphorus screen in front of the EBSD detector was set to 15±0.1mm. The acquisition and post-processing of EBSD data was performed with HKL Channel 5 software. For EBSD analysis the austenite (fcc) phase was selected from the HKL database for all samples because no ferrite (bcc) phase was expected to exist in the base 316H material.

3. Results

3.1. Residual intergranular strains

3.1.1 Parent material specimens

For conciseness we will report only the longitudinal strains in this paper: the full data are presented elsewhere [30]. Figure 2 shows the development of the intergranular strains between the different grain families as a function of the level of pre-strain, and the associated change in diffraction peak width. The peak width in

diffraction patterns can provide a qualitative comparison of the dislocation densities, and provide a proxy measurement of the degree of plastic deformation [24]. The peak width is a convolution of the instrumental and inherent material peak widths with changes in width caused by microstructural effects that are introduced by plastic deformation. The trend linking plastic deformation and residual intergranular strains as seen in figure 2a was previously observed by Peng *et al.* [18].

The anisotropy strain ε_A was calculated from the residual strains on 200 and 111 planes at 45°(LD) according to:

$$\varepsilon_{h00} - \varepsilon_{hkl} = A_{hkl} \times \varepsilon_A \qquad \text{Eq. (1)}$$

where ε_{hkl} is the intergranular strain on *hkl* plane and A_{hkl} is the anisotropy factor describing the degree of variation of the crystal stiffness with orientation.

The 111 and 200 planes were selected because these planes represent the extremes of elastic stiffness in stainless steel. The variation of anisotropy strain with plastic deformation is given in Figure 3. A linear fit was made for use in predicting the plastic deformation in the cross-weld specimens.

3.1.2 Cross-weld specimens

The variation of residual strains as a function of angular direction from the pipe longitudinal direction (LD, at 45˚ to the incident beam) to the hoop direction (HD, at 135˚ to the incident beam) is plotted for the cross-weld specimen with zero pre-strain at 7 and 29 mm away from the weld centre in Figure 4. The effect of welding on the residual strains on the different *hkl* planes appears to be low and no systematic trends could be discerned. The peak widths at 7 mm distance are shown in

figure 5 to allow comparison with the data from the pre-strained tubes. The peak widths did not vary with direction, which is predictable as the effects of plastic strain on the microstructure are not direction-dependent.

The variation of residual strains as a function of sample direction from LD (45°) to HD (135°) is plotted in Figure 6 for the specimen welded after 20% pre-strain at 7, 12, and 29 mm away from the weld centre. The effect of the pre-straining is most evident in figure 6c, at 29 mm from the weld. At 7 mm, close to the weld, the effect of the pre-straining has effectively been annealed by the heat input from the welding (figure 6a). Tensile strains accumulate on the 200 plane in the longitudinal direction, becoming compressive as the orientation progresses to the hoop direction. The corresponding peak widths are shown in figure 7 at 7 and 29 mm, showing that the plastic deformation has increased the diffraction peak width far from the weld.

The variation of anisotropy strain along the length of the welded specimens with 0 and 20% prior deformation is given in Figure 8a. This shows again the effective annealing of the intergranular strains, generated by the prior plastic deformation, from the heat from the welding operation.

3.3. Crystallographic texture

Parent specimen

The 111, 100, 110 and 311 pole figures obtained by neutron diffraction are given in Figure 9. There is some 111 texture in the LD and 110 texture in the radial direction (RD) before the deformation, as a consequence of the tube drawing process. The 111 texture in the LD increases with increasing deformation and reaches 8×

random after 25% deformation but there is no change in either the HD or RD (Figure 9a). There is also texture development for the 100 plane in the LD direction with increasing plastic deformation although it is small (2× random, Figure 9b). This type of texture is a duplex <111> and <100> fibre texture.

For the 110 plane a small texture develops in the RD and HD, but it is not affected in the LD although the reflection for this plane is weak compared to HD and RD (Figure 9c). There is no significant texture evolution for the 311 plane with increasing deformation apart from a small change in LD after 10% deformation (Figure 9d).

Cross-weld specimen

Figure 10 shows the texture after welding onto 20% plastically strained material: the figure shows the pole figures for the four selected grain families at a distance of 4.6 mm from the weld centre-line. Data obtained from 7 mm onwards from the weld centre-line were essentially unchanged from the as-strained material. Since the temperature of the molten weld metal is very high (<1400°C) the grains near the fusion boundary are likely to be subjected to recovery and/or recrystallization and hence have a random orientation.

3.4. Low angle boundaries

Parent specimen

The distribution of low-angle boundaries (LABs) for the specimens deformed up to 25% plastic deformation is given in Figure 11. Boundaries are defined according to the misorientation angle between two adjacent points. For fcc metallic alloys, any

misorientation angle greater than 15° is considered as a high-angle grain boundary and a misorientation angle between 3°-15° is taken as a low-angle boundary (LAB) [31], [32]. In Figure 11, it is clearly seen that the distribution of LABs increases as the plastic deformation increases. The LABs are mostly concentrated near grain boundaries at small deformation (Figure 11(a-d)); however, it is observed that at higher deformation LABs also appear inside the grains owing to the dislocation bands and arrays (Figure 11(e)). In a grain, as the deformation proceeds, dislocations intersect each other and start to lose their mobility, i.e. strain hardening begins. With further plastic deformation they begin to pile-up near grain boundaries and form bands and arrays inside the grains [33]. The fractions of the frequency of LABs (3-15°) to the total of all misorientation angles in the sampling areas were calculated and are presented in Figure 12. It is seen that the fraction of LABs increases almost linearly with increasing plastic deformation.

Cross-weld specimen

The variation of LAB fraction as a function of distance away from the weld centre-line on the LD-RD surface of the specimen welded after 20% deformation is given in Figure 13 (note that no direction-dependence in LAB population was observed). It is seen that the LAB fraction decreases approaching the weld fusion boundary. Each point represents LAB fraction which was determined in an area of $300 \times 900\ \mu m^2$ (height × width) in the mid-height of the surface.

4. Discussion

4.1 Development of residual strains with plastic deformation

In this study, the measurements of intergranular residual strains have shown that tensile strains were accumulated on the 200 and 311 planes, and compressive strains exist on the 111 and 220 planes. Similar results were reported in [18] for AISI 304 austenitic stainless steel subjected to intermediate levels of plastic deformation up to 44.7%, and in [17] for AISI 316H austenitic stainless steel subjected to 3% plastic deformation. Larsson *et al.* [22] claimed that there are two origins of the residual intergranular strains, which are elastic anisotropy and strain redistribution due to slip along preferred systems: they also stated that it is difficult to distinguish their relative contributions. The sign of the intergranular strains can be explained with different elastic stiffness of the planes, i.e. elastic anisotropy. Daymond and Bouchard [17] reported the elastic stiffness of 111, 220, 311 and 200 planes in the loading direction as 245, 210, 180 and 150 GPa, respectively. The 111 plane is the stiffest whereas the 200 plane is the least stiff. This indicates that when the specimen is unloaded, owing to the elastic equilibrium between the grains, the less stiff planes, i.e. 200 and 311, retain tensile strain whereas the stiffer planes, i.e. 111 and 220, sustain compressive strains.

Deformation mechanisms also have an influence on the residual strains. Slip along preferred crystallographic directions and planes may cause strain redistribution among the grains. Feaugas *et al.* [34] explain how the stress/strain is redistributed between the grains and inside the grains during the deformation of 316L stainless steel. For austenitic stainless steel, owing to its low stacking fault energy, planar slip is observed and cross-slip is prevented. The grain boundaries act as strong barriers to slip. At the beginning of plastic deformation (<1.5%) dislocations pile up near grain boundaries and that imposes a stress concentration near the

boundary, i.e. intergranular stresses. Therefore, increasing plastic strain during the early stages of deformation results in a higher stress concentration near the grain boundaries because the number of dislocations in the pile-up increases. Intergranular stresses start to decrease with the activation of multiple slip and cross-slip: the intergranular stresses are relaxed and the plastic strain compatibility is maintained between the grains. Slip transmission across grain boundaries and activation of dislocation sources in neighbouring grains also reduce the intergranular stresses. Further deformation after the activation of cross-slip and multiple slip produces heterogeneous dislocation structures like dislocation bands and arrays of dislocations inside the grains: therefore, intragranular stresses increase. It was reported that the difference between inter- and intra-granular stresses becomes zero at about 6% plastic deformation [34]. Note that, as discussed in the literature [15], [17], [18], [21], [22], [35], the term "residual intergranular strains" was preferred to be used to define the residual strains measured with neutron diffraction because the intragranular strains were thought to be negligible. However, Feaugas's explanation suggests that the intragranular strains cannot be neglected because they are as significant as the intergranular strains after 6% deformation. It can be concluded that the residual strain measured with neutron diffraction after plastic deformation beyond 6% deformation is composed of: (1) intergranular strains which arise owing to the elastic anisotropy of the different *hkl* planes; and (2) intragranular strains which arise owing to the heterogeneous dislocation structures inside the grains.

Larsson *et al.* [22] found that the initial texture has an influence on the residual strain distribution. He observed that the strain distribution becomes more complex

after the deformation of an austenitic stainless steel with an initial texture of 1.6 × random. In the present study, a 3×random texture was found before deformation for the 111 plane family in the loading direction (Figure 9). Therefore, this might have influenced the residual strain distribution. The texture in specimens deformed up to 25% plasticity (Figure 9) suggests that a duplex <111> and <100> fibre texture forms before 10% deformation and becomes stronger as the deformation proceeds. The intensity ratio of <111> to <100> is about 3.5 after 25% plastic deformation. Such a duplex texture is often observed in fcc materials subjected to axisymmetric flow and the ratio of the polar intensity varies with the stacking fault energy of the material [27]. A high volume fraction of grains oriented in <111> and <100> directions parallel to the loading direction would influence the generation of residual strains. The low strain level on the 111 plane can be explained by the fact that a high number of grains are oriented in the <111> direction parallel to the pre-straining direction as well as the high stiffness of the 111 direction. Similarly, high strains on the 200 plane can be attributed to the increasing number of grains oriented with the <100> direction parallel to the pre-straining direction and the low stiffness of the 200 plane.

4.2 Evaluation of plastic deformation using anisotropy strain

Daymond *et al.* [12] used residual strains to predict the plastic deformation via anisotropy strain. Their technique requires a calibration curve similar to Figure 3. The data in figure 3 were used as a calibration to predict the plastic deformation in the welded specimens with 0% and 20% prior deformation from the distribution of anisotropy strains presented in Figure 8a. The prediction of plastic strain is given in Figure 8b. The slight increase of plastic deformation in the base metal of the un-

deformed specimen can be attributed to the cyclic hardening due to the double-pass welding. In the 20% pre-strained sample it is seen that plastic deformation in this specimen is decreasing closer to the weld. This can be explained by partial recovery as a consequence of the heat input during welding.

4.3 Evaluation of plastic deformation using diffraction peak widths

According to Feaugas's explanation of inter- and intra-granular strains, it can be concluded that the plastic deformation can be tracked with the dislocation density and structures such as pile-ups near grain boundaries and heterogeneous dislocation structures inside the grains [34]. Diffraction peak width measurements (Figure 2b) by neutron diffraction suggest that dislocation density increases with increasing deformation for any *hkl* plane in any specimen direction: furthermore Lewis and Truman [26] indicated that the peak broadening is insensitive to the diffraction vector direction. Therefore, it is a measure of equivalent plastic strain. The peak widths as a function of plastic strain are given in figure 2b.

The peak widths for the welded specimens with 0% and 20% prestrain are shown in Figure 14 (a) and (b) respectively. The corresponding predicted plastic deformation at different positions from the weld centre-line for specimens welded after 0% and 20% prior deformation, using the averaged peak widths, is given in Figure 15. The plastic deformation in the underformed specimen is almost zero when data from the 200 and 311 planes are used. However, the 111 plane gives ~1% deformation at 12 mm. Cyclic hardening owing to the double-pass welding might have increased the dislocation density in that region.

4.4 Prediction of plastic deformation using EBSD

Dislocation structures such as pile-ups near grain boundaries and heterogeneous dislocation structures inside grains can be detected by EBSD as the presence of these structures results in small misorientations: i.e., low-angle boundaries (LABs) [36]. LAB fraction is useful to quantify the changes in misorientations with increasing plastic deformation. Figure 12 shows that the LAB fraction varies almost linearly with increasing plastic deformation. This linearity was used as a calibration to determine the variation of plastic deformation in the specimen which was 20% prestrained before welding. The prediction of plastic deformation by using LAB fraction is given in Figure 16. Rearrangement of dislocations and partial annihilation occur as a result of heat dissipated during welding; therefore, the misorientations produced by the pile-ups near grain boundaries and heterogeneous dislocation structures inside grains are affected. The trend in Figure 16 is similar to the prediction obtained using the anisotropy strains in Figure 8b and using the peak widths in Figure 15.

4.5 Prediction of plastic deformation using hardness

For hardness measurements, the surface of the sample was ground and polished. The hardnesses of the base material with 0%, 10% and 20% pre-strain are 154, 218 and 251 H_V, respectively. In these measurements 5kgf was used.

Assuming a linear increase in hardness with plastic deformation, hardness measurements on the cross-weld samples can be used to predict the plastic deformations as shown in Figure 17.

4.6 Comparison of the plastic deformation predictions

A comparison of plastic deformation predictions using the various techniques is given in Figure 18. It is seen that there is a good agreement in the trends of the different prediction methods. EBSD and hardness predict almost the same value at ~5mm from WCL. Similarly, the predictions of neutron diffraction (ND) peak width and hardness at ~9mm from WCL are comparable. There is more deviation for the neutron diffraction and EBSD predictions: but note that EBSD and hardness are surface measurements and neutron diffraction is a bulk measurement. The dislocation density may vary in the neutron gauge volume because of the double pass welding process. It is also difficult to differentiate the broadening effects of plastic deformation from those due to local material variations during welding process. Predicted values of plastic strain using the anisotropy strain derived from the neutron diffraction data are generally lower than that of the other methods.

It is seen that EBSD predicts about 1-4% more plastic strain relative to the prediction based on hardness measurements. For EBSD measurements a conventional surface preparation technique, which included grinding and polishing, was used. It is possible that the surface grinding might have altered the dislocation structure on the sample surface, which resulted in a higher plastic deformation prediction.

Conclusions

Neutron diffraction has been used to measure the intergranular strain developed in 316H austenitic stainless steel as a consequence of plastic deformation and subsequent welding operations.

1. As the material is deformed plastically, significant intergranular residual strains develop in the loading direction owing to the elastic anisotropy and strain redistribution due to slip along preferred systems.

2. The proportion of low-angle grain boundaries was seen to increase as the degree of plastic deformation was increased.

3. Texture results showed that the 111 and 200 planes are re-oriented perpendicular to the pre-straining direction with increasing plastic deformation. The strongest tensile strains develop on the 200 plane since it is more compliant compared to the 111 plane.

4. Anisotropy strain was calculated using the residual strains from the different diffracting grains as a function of increasing plastic deformation. Similarly the increase in diffraction peak width with plastic deformation was measured. These measures, along with the low-angle grain boundary fraction and the material hardness, were used to provide predictions of the prior plastic strain in a sample welded after deformation. Good agreement was seen between the various measures.

5. The welding process reduced the apparent plasticity owing to the thermal cycle and consequent annealing effect. The effect was seen to be consistent across all the proxy measures of plastic strain that were studied here.

Acknowledgements

MOA is grateful for funding from EDF Energy (formerly British Energy) and Dr M. Spindler is thanked for his support. We are grateful for the provision of neutron

beam-time at the STFC ISIS facility in the UK and at the FRM-II facility in Munich; and Dr A. Paradowska and Dr M. Hofmann are thanked for experimental support.

MEF is grateful for funding from the Lloyd's Register Foundation, a charitable foundation helping to protect life and property by supporting engineering-related education, public engagement and the application of research.

References

[1] ASME, *Boiler and Pressure Vessel Code, Section I: Rules for Construction of Power Boilers*. New York, USA, 2010.

[2] M. O. Speidel and R. M. Magdowski, "Stress corrosion cracking of nuclear reactor pressure vessel and piping steels," *Int. J. Press. Vessel. Pip.*, vol. 34, no. 1, pp. 119–142, 1988.

[3] C. García, F. Martín, P. D. Tiedra, J. . Heredero, and M. . Aparicio, "Effects of prior cold work and sensitization heat treatment on chloride stress corrosion cracking in type 304 stainless steels," *Corros. Sci.*, vol. 43, no. 8, pp. 1519–1539, 2001.

[4] S. Yamazaki, Z. Lu, Y. Ito, Y. Takeda, and T. Shoji, "The effect of prior deformation on stress corrosion cracking growth rates of Alloy 600 materials in a simulated pressurized water reactor primary water," *Corros. Sci.*, vol. 50, no. 3, pp. 835–846, 2008.

[5] S. Ghosh and V. Kain, "Effect of surface machining and cold working on the ambient temperature chloride stress corrosion cracking susceptibility of AISI 304L stainless steel," *Mater. Sci. Eng. A*, vol. 527, no. 3, pp. 679–683, 2010.

[6] L. Fournier, M. Savoie, and D. Delafosse, "Influence of localized deformation on A-286 austenitic stainless steel stress corrosion cracking in PWR primary water," *J. Nucl. Mater.*, vol. 366, no. 1, pp. 187–197, 2007.

[7] B. Wilshire and M. Willis, "Mechanisms of strain accumulation and damage development during creep of prestrained 316 stainless steels," *Metall. Mater. Trans. A*, vol. 35, no. 2, pp. 563–571, 2004.

[8] M. Willis, A. McDonaugh-Smith, and R. Hales, "Prestrain effects on creep ductility of a 316 stainless steel light forging," *Int. J. Press. Vessel. Pip.*, vol. 76, no. 6, pp. 355–359, 1999.

[9] A. H. Sherry, "Advances and Challenges in Structural Integrity," *Appl. Mech. Mater.*, vol. 7–8, pp. 13–22, 2007.

[10] P. Marshall, *Austenitic stainless steels: microstructure and mechanical properties*. Springer Science & Business Media, 1984.
[11] Q. Auzoux, L. Allais, C. Caës, I. Monnet, A. F. Gourgues, and A. Pineau, "Effect of pre-strain on creep of three AISI 316 austenitic stainless steels in relation to reheat cracking of weld-affected zones," *J. Nucl. Mater.*, vol. 400, no. 2, pp. 127–137, 2010.
[12] M. R. Daymond, M. A. M. Bourke, R. B. Von Dreele, B. Clausen, and T. Lorentzen, "Use of Rietveld refinement for elastic macrostrain determination and for evaluation of plastic strain history from diffraction spectra," *J. Appl. Phys.*, vol. 82, no. 4, pp. 1554–1562, 1997.
[13] D. J. Smith, R. H. Leggatt, G. A. Webster, H. J. Macgillivray, P. J. Webster, and G. Mills, "Neutron diffraction measurements of residual stress and plastic deformation in an aluminium alloy weld," *J. Strain Anal. Eng. Des.*, vol. 23, no. 4, pp. 201–211, 1988.
[14] M. Kamaya, A. J. Wilkinson, and J. M. Titchmarsh, "Measurement of plastic strain of polycrystalline material by electron backscatter diffraction," *Nucl. Eng. Des.*, vol. 235, no. 6, pp. 713–725, 2005.
[15] M. R. Daymond, "Internal Stresses in Deformed Crystalline Aggregates," *Rev. Mineral. Geochemistry*, vol. 63, no. 1, p. 427 LP-458, Nov. 2006.
[16] M. T. Hutchings, P. J. Withers, T. M. Holden, and T. Lorentzen, *Applications to Problems in Materials Science and Engineering*. CRC Press, 2005.
[17] M. R. Daymond and P. J. Bouchard, "Elastoplastic deformation of 316 stainless steel under tensile loading at elevated temperatures," *Metall. Mater. Trans. A*, vol. 37, no. 6, pp. 1863–1873, 2006.
[18] R. Lin Peng, M. Odén, Y. . Wang, and S. Johansson, "Intergranular strains and plastic deformation of an austenitic stainless steel," *Mater. Sci. Eng. A*, vol. 334, no. 1, pp. 215–222, 2002.
[19] J. D. Verhoeven, *Fundamentals of physical metallurgy*. New York : Wiley, 1975.
[20] M. E. Fitzpatrick and A. Lodini, *Analysis of Residual Stress by Diffraction Using Neutron and Synchrotron Radiation*, vol. 14, no. 9. 2003.
[21] J. W. L. Pang, T. M. Holden, J. S. Wright, and T. E. Mason, "Generation of intergranular strains in 309H stainless steel under uniaxial loading," *Acta Mater.*, vol. 48, no. 5, pp. 1131–1140, 2000.
[22] C. Larsson, B. Clausen, T. M. Holden, and M. A. M. Bourke, "Measurements and predictions of strain pole figures for uniaxially compressed stainless steel," *Scr. Mater.*, vol. 51, no. 6, pp. 571–575, 2004.
[23] E.-W. Huang *et al.*, "Plastic behavior of a nickel-based alloy under monotonic-tension and low-cycle-fatigue loading," *Int. J. Plast.*, vol. 24, no. 8, pp. 1440–1456, 2008.
[24] M. Kamaya, A. J. Wilkinson, and J. M. Titchmarsh, "Quantification of plastic strain of stainless steel and nickel alloy by electron backscatter diffraction," *Acta Mater.*, vol. 54, no. 2, pp. 539–548, 2006.
[25] A. M. Korsunsky, M. R. Daymond, and K. E. James, "The correlation between plastic strain and anisotropy strain in aluminium alloy polycrystals," *Mater. Sci. Eng. A*, vol. 334, no. 1, pp. 41–48, 2002.

[26] S. J. Lewis and C. E. Truman, "Diffraction measurements for evaluating plastic strain in A533B ferritic steel—a feasibility study," *J. Phys. D. Appl. Phys.*, vol. 43, no. 26, p. 265501, 2010.
[27] X.-L. Wang *et al.*, "Inter-and intragranular stresses in cyclically-deformed 316 stainless steel," *Mater. Sci. Eng. A*, vol. 399, no. 1, pp. 114–119, 2005.
[28] M. R. Daymond, J. A. James, L. Edwards, and J. R. Santisteban, "ENGIN-X: a third-generation neutron strain scanner," *J. Appl. Crystallogr.*, vol. 39, no. 6, pp. 812–825, 2006.
[29] S. I. Campbell, F. A. Akeroyd, and C. M. Moreton-Smith, "Open GENIE – Analysis and Control .," no. November 2002, 2002.
[30] M. O. Acar, "Effects of plastic strain history on the properties of stainless steel boiler tube welds," The Open University, 2012.
[31] M. Preuss, P. J. Withers, J. W. L. Pang, and G. J. Baxter, "Inertia welding nickel-based superalloy: Part I. Metallurgical characterization," *Metall. Mater. Trans. A*, vol. 33, no. 10, pp. 3215–3225, 2002.
[32] D. Dingley, "Progressive steps in the development of electron backscatter diffraction and orientation imaging microscopy," *J. Microsc.*, vol. 213, no. 3, pp. 214–224, Feb. 2004.
[33] G. E. Dieter, *Mechanical metallurgy*. London: McGraw-Hill Book Company, 1988.
[34] X. Feaugas, "On the origin of the tensile flow stress in the stainless steel AISI 316L at 300 K: back stress and effective stress," *Acta Mater.*, vol. 47, no. 13, pp. 3617–3632, 1999.
[35] J. Q. Da Fonseca, E. C. Oliver, P. S. Bate, and P. J. Withers, "Evolution of intergranular stresses during in situ straining of IF steel with different grain sizes," *Mater. Sci. Eng. A*, vol. 437, no. 1, pp. 26–32, 2006.
[36] P. S. Bate, R. D. Knutsen, I. Brough, and F. J. Humphreys, "The characterization of low-angle boundaries by EBSD.," *J. Microsc.*, vol. 220, no. Pt 1, pp. 36–46, Oct. 2005.
[37] F. Di Gioacchino, and J. Quinta da Fonseca, *An experimental study of the polycrystalline plasticity of austenitic stainless steel*, International Journal of Plasticity 74 (2015), pp. 92-109.
[38] Y.B. Das, A.N. Forsey, T.H. Simm, K.M. Perkins, M.E. Fitzpatrick, S. Gungor, and R.J. Moat, *In situ observation of strain and phase transformation in plastically deformed 301 austenitic stainless steel*, Materials & Design 112 (2016), pp. 107-116.

Figure(s)

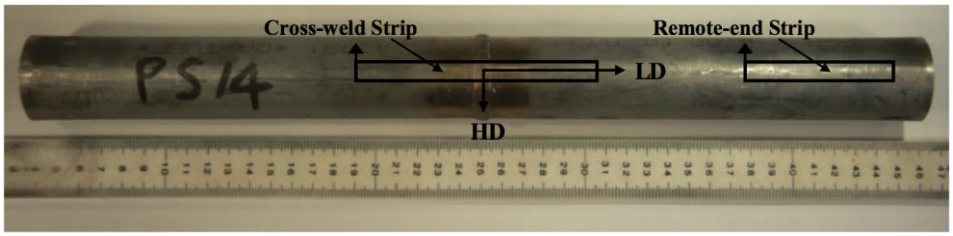

Figure 1 Position of the cross-weld and remote-end strips extracted from the welded tubes. (LD is the longitudinal direction of the tube, parallel to the pre-straining direction; HD is the hoop direction of the tube perpendicular to the pre-straining direction; RD (into the page) is the radial direction of the tube perpendicular to the pre-straining direction)

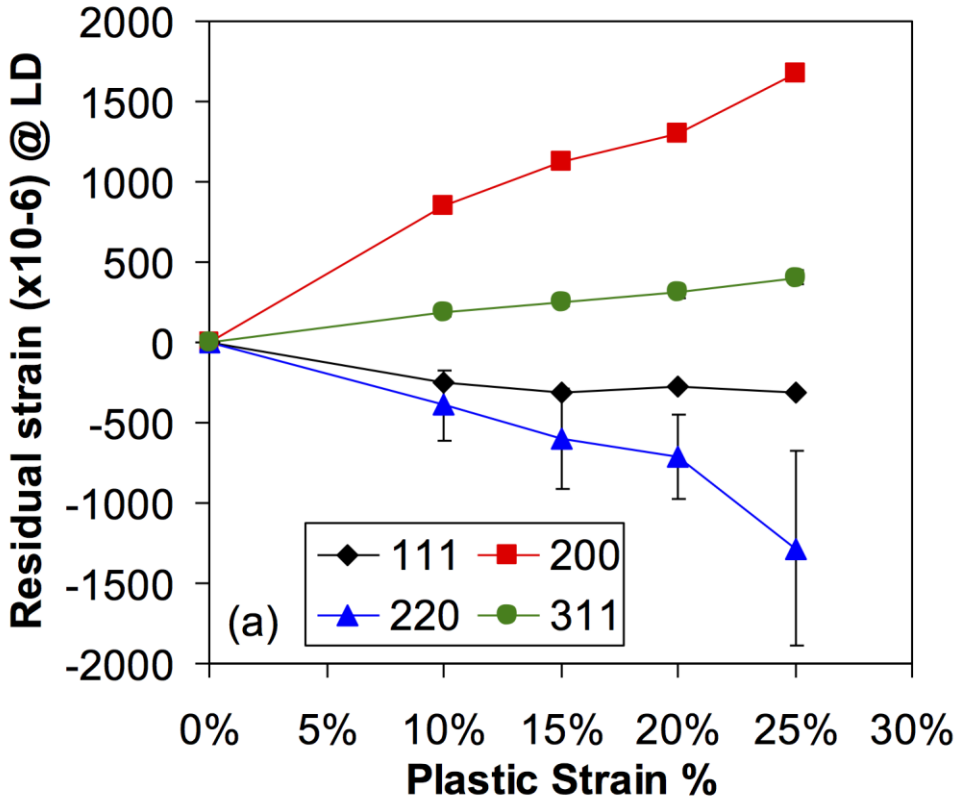

(a)

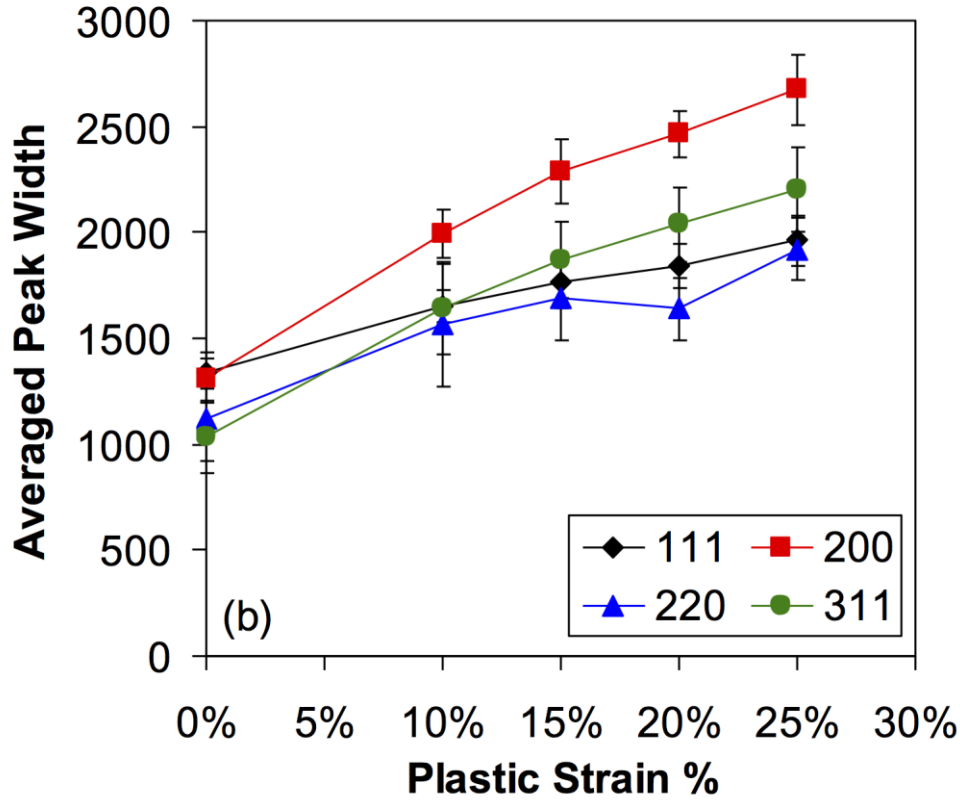

(b)

Figure 2 (a) The development of residual intergranular strains on *hkl* planes at LD (longitudinal direction of the tube) with increasing plastic deformation; and (b) corresponding peak widths as an average of the measurements at different sample directions.

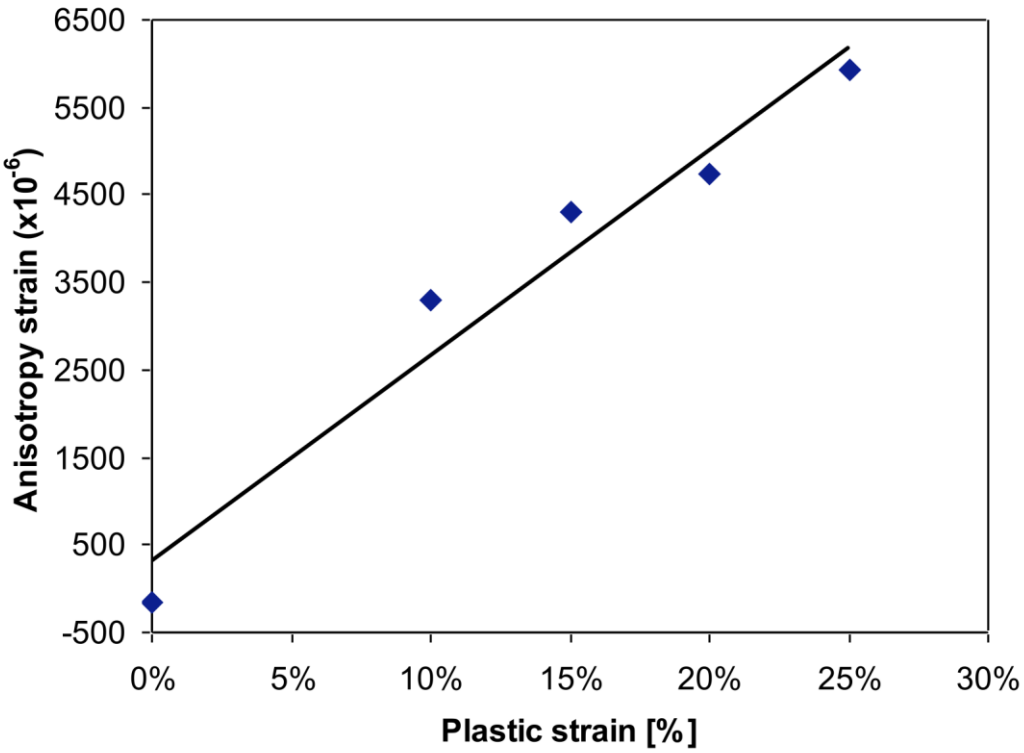

Figure 3 The variation of anisotropy strain (ε_{200} - $\varepsilon_{111} = A_{111}\varepsilon_A$) with plastic deformation. Note that ε_{200} and ε_{111} are the residual strains at 45°(LD).

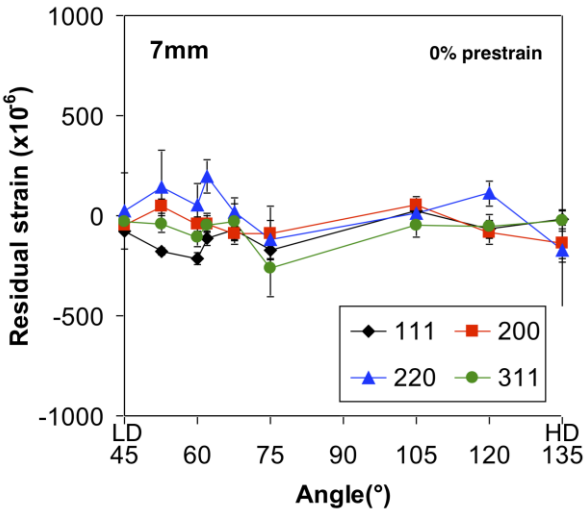

(a)

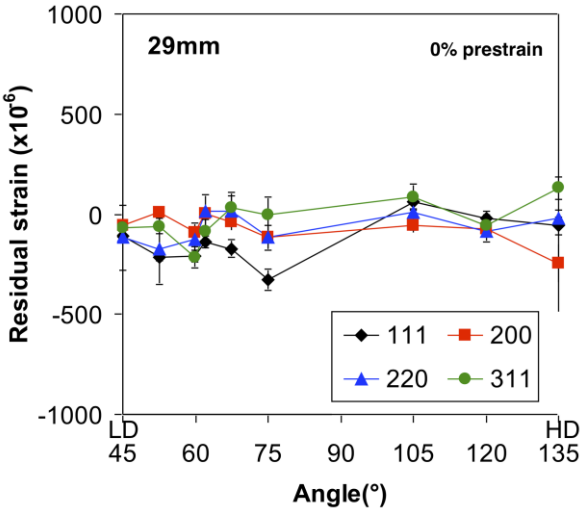

(b)

Figure 4 Residual intergranular strains, as a function of direction (expressed as angle relative to the incident neutron beam, 45° to 135° equivalent to strains LD to HD) for the cross-weld sample with zero pre-strain at (a) 7 and (b) 29mm away from the weld centre line.

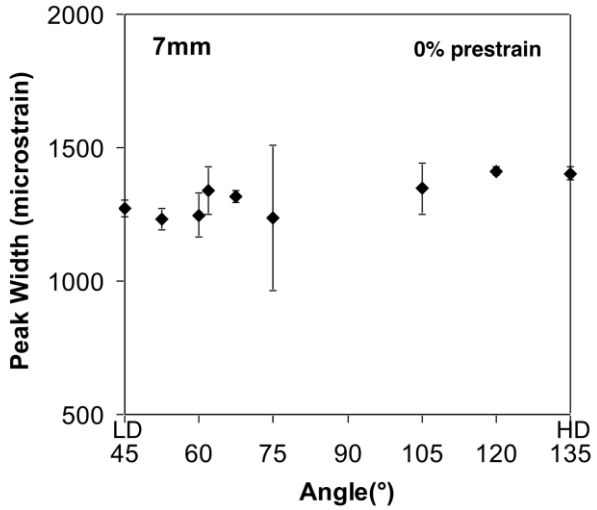

Figure 5 Diffraction peak width, expressed as effective microstrain, for the zero pre-strain sample at 7 mm from the weld centre line

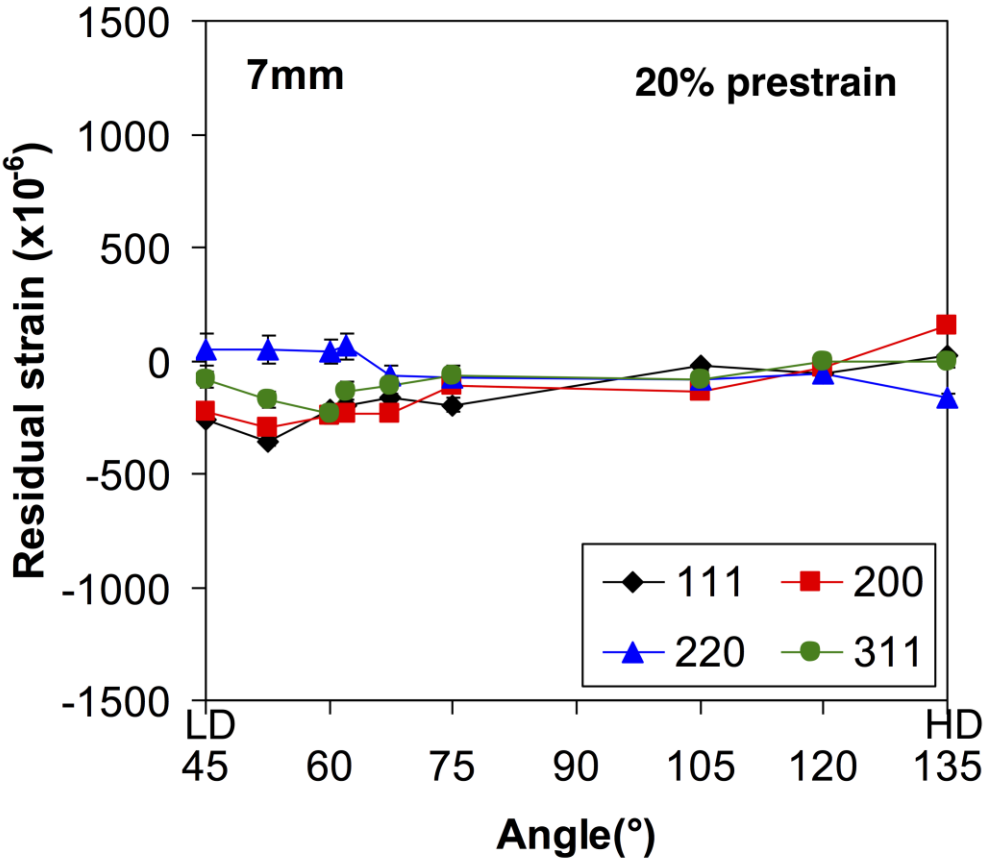
7mm
20% prestrain
Residual strain (x10-6)
1500
1000
500
0
-500
-1000
-1500
111
200
220
311
LD
HD
45
60
75
90
105
120
135
Angle(°)

6(a)

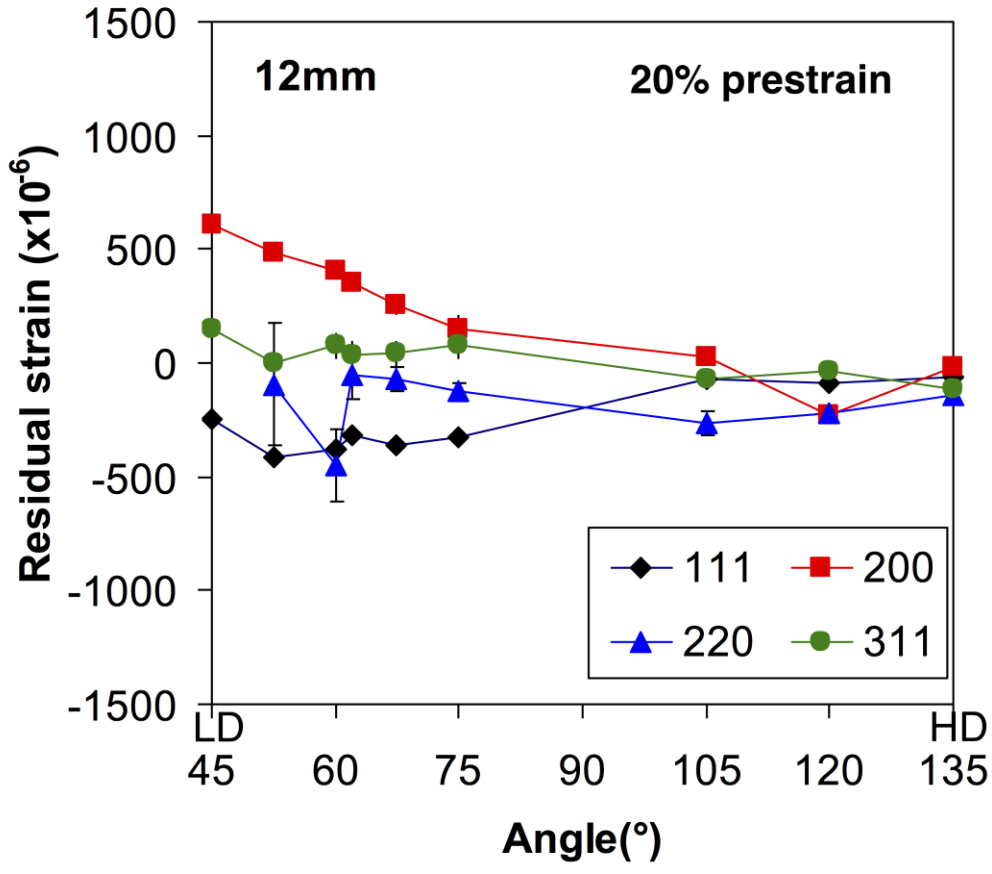
12mm
20% prestrain
Residual strain (x10-6)
1500
1000
500
0
-500
-1000
-1500
111
200
220
311
LD
HD
45
60
75
90
105
120
135
Angle(°)

6(b)

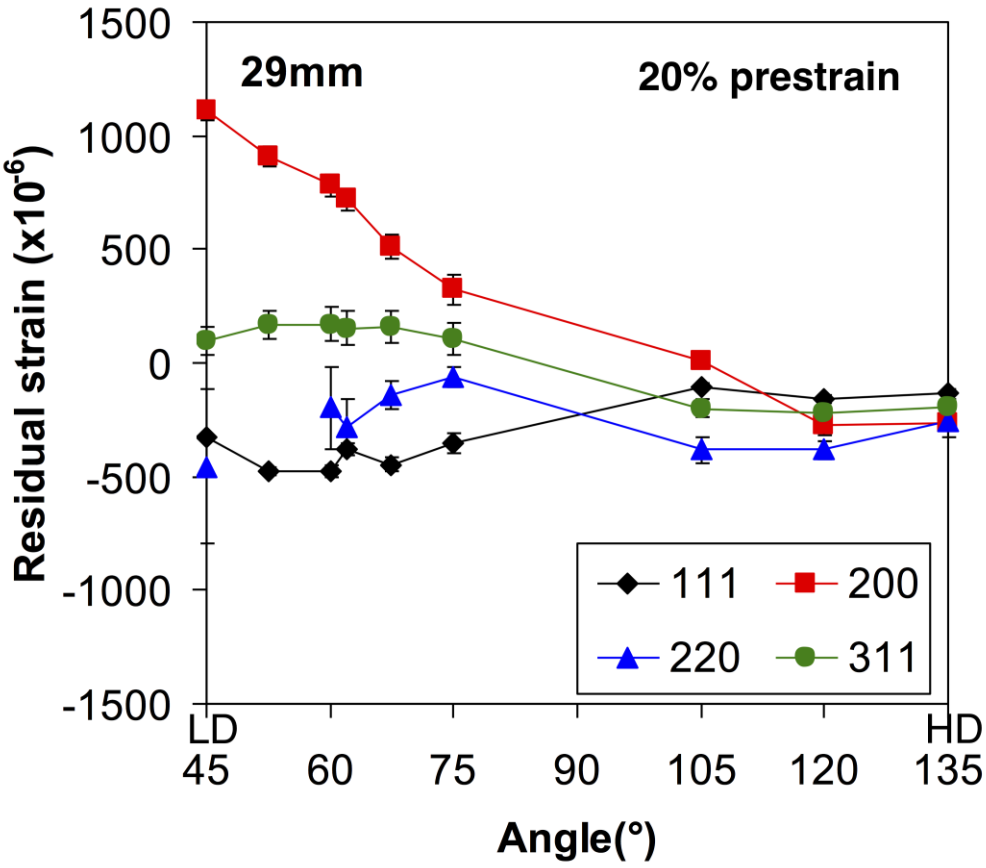

6(c)

Figure 6 Residual intergranular strains for the cross-weld sample with 20% pre-strain at (a) 7, (b) 12 and (c) 29mm away from the weld centre line.

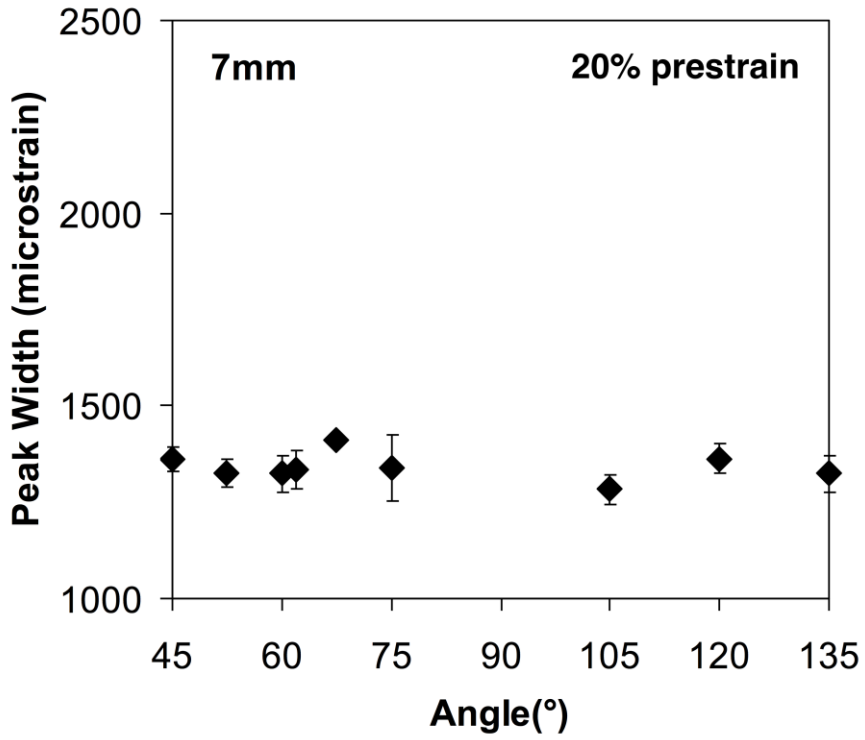

(a)

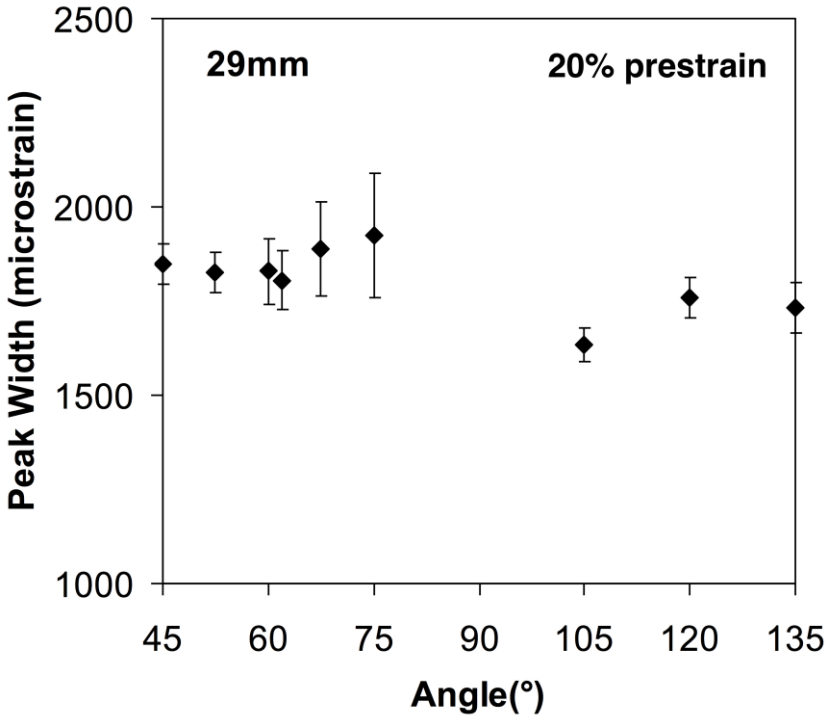

(b)

Figure 7 Diffraction peak width, expressed as effective microstrain, for the 20% pre-strain sample at (a) 7 and (b) 29 mm from the weld centre line

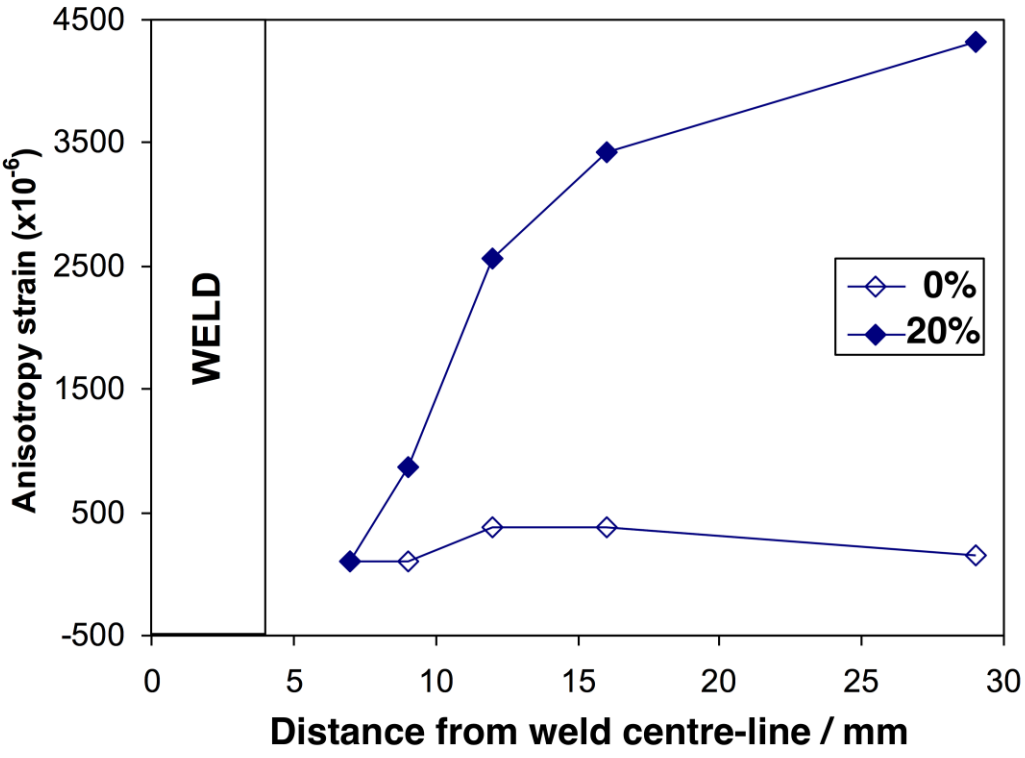

(a)

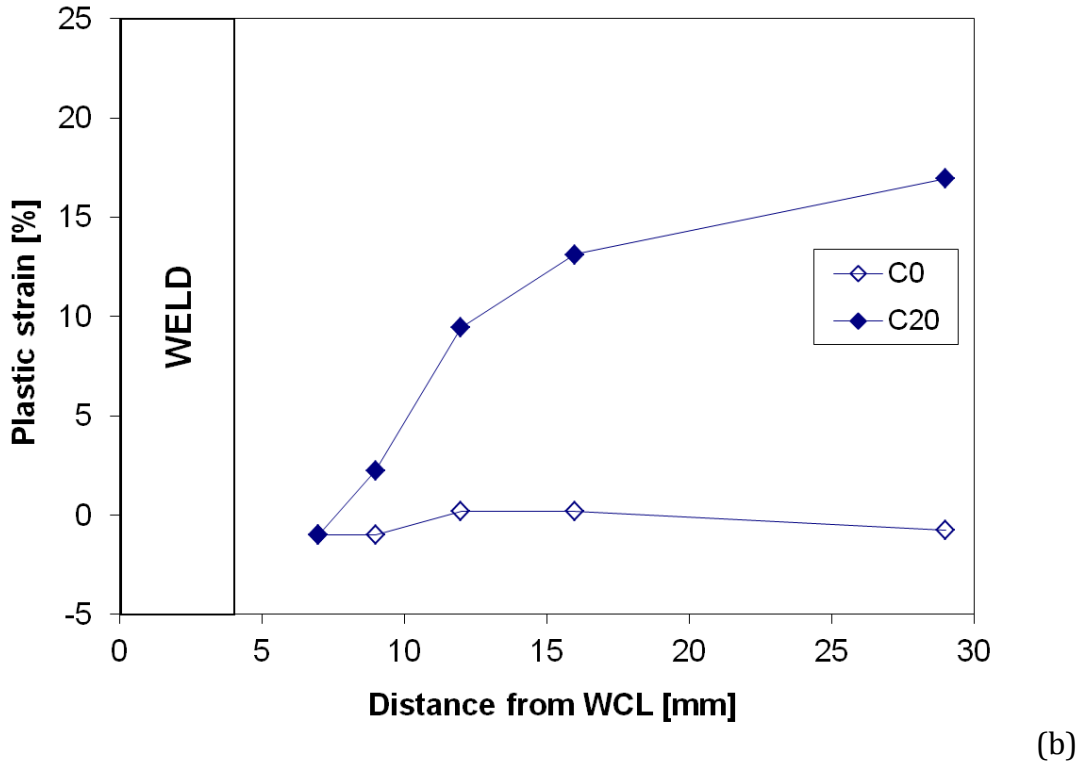

(b)

Figure 8 (a) The variation of anisotropy strain (ε_{200} - $\varepsilon_{111} = A_{111}\varepsilon_A$) along the cross-weld specimens with zero and 20% pre-strain. Note that ε_{200} and ε_{111} are the residual strains at 45°(LD). (b) Corresponding plastic strain predicted by using Figure 3.

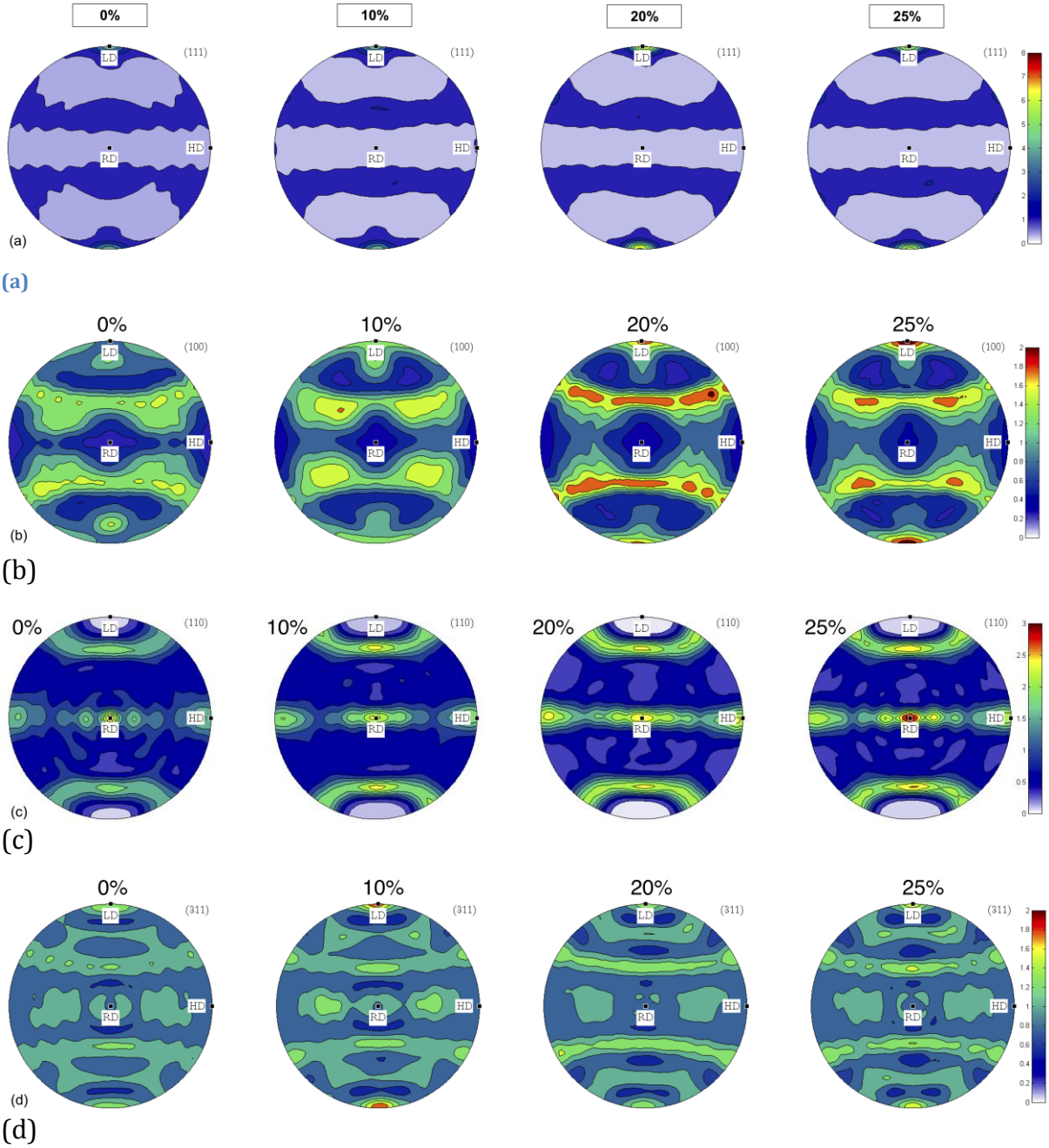

Figure 9: Pole figures of 111 (a), 100 (b), 110 (c) and 311 (d) planes showing the development of crystallographic texture in the parent material after 0, 10, 20 and 25% plastic deformation. (LD: longitudinal direction of the tube, HD: hoop direction, RD: radial direction)

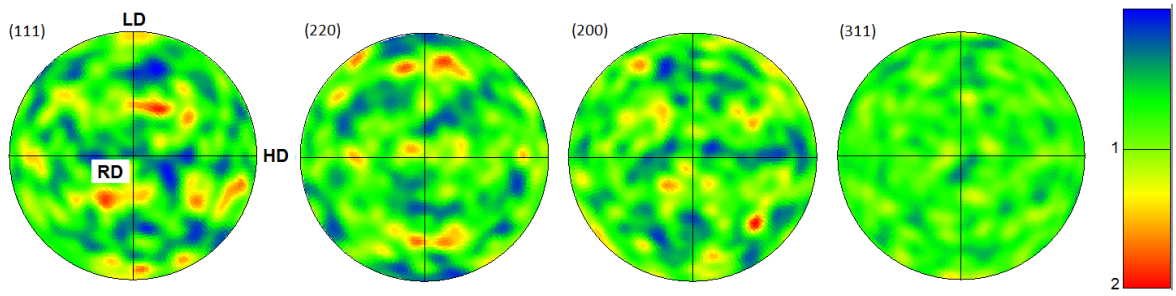

Figure 10: 111, 220, 200 and 311 pole figures for 20% pre-strain cross-weld sample obtained by EBSD from 7 mm away from WCL. (LD: longitudinal direction of the tube, HD: hoop direction, RD: radial direction)

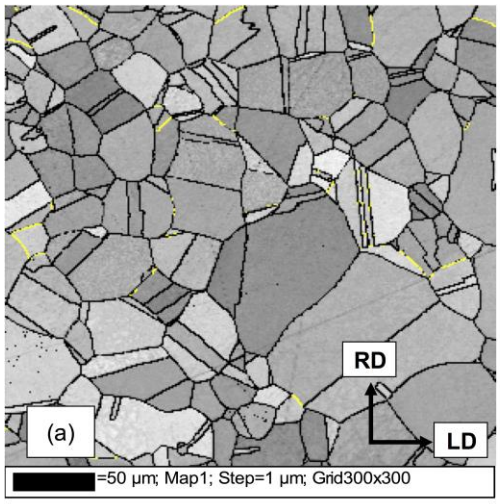
RD
LD
(a)
=50 µm; Map1; Step=1 µm; Grid300x300

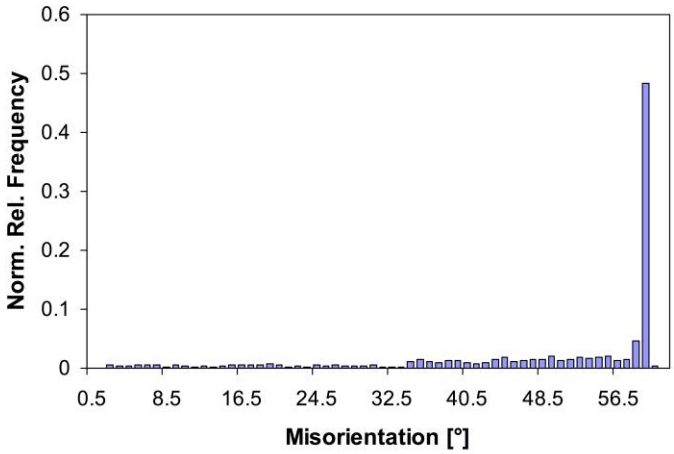
Norm. Rel. Frequency
0.6
0.5
0.4
0.3
0.2
0.1
0
0.5
8.5
16.5
24.5
32.5
40.5
48.5
56.5
Misorientation [°]

(11a)

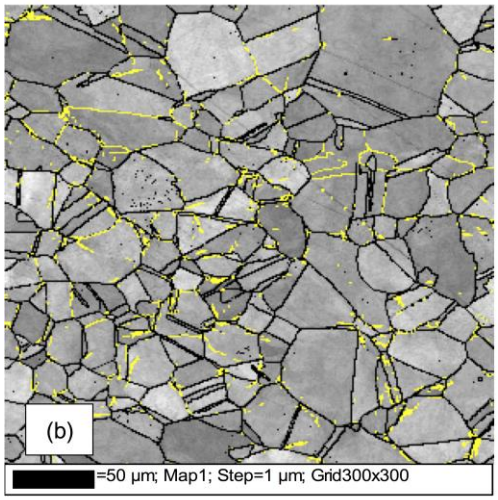
(b)
=50 µm; Map1; Step=1 µm; Grid300x300

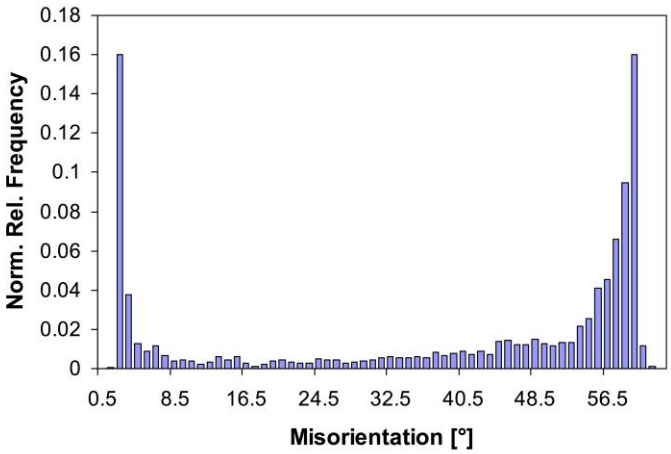
Norm. Rel. Frequency
0.18
0.16
0.14
0.12
0.1
0.08
0.06
0.04
0.02
0
0.5
8.5
16.5
24.5
32.5
40.5
48.5
56.5
Misorientation [°]

(11b)

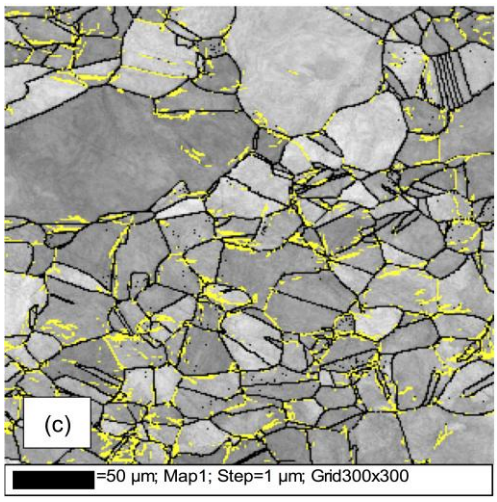
(c)
=50 µm; Map1; Step=1 µm; Grid300x300

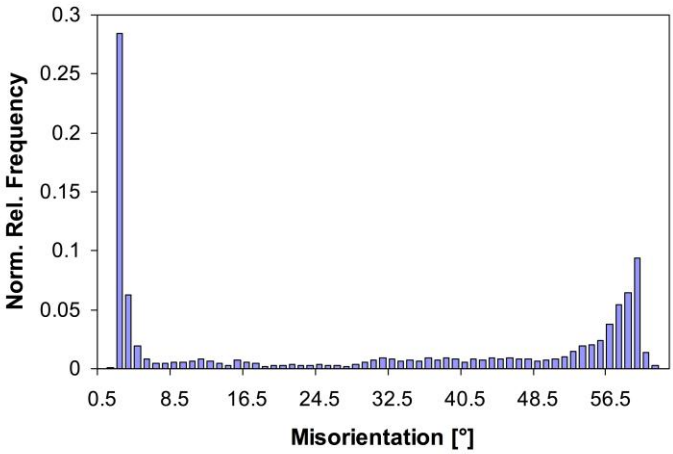
Norm. Rel. Frequency
0.3
0.25
0.2
0.15
0.1
0.05
0
0.5
8.5
16.5
24.5
32.5
40.5
48.5
56.5
Misorientation [°]

(11c)

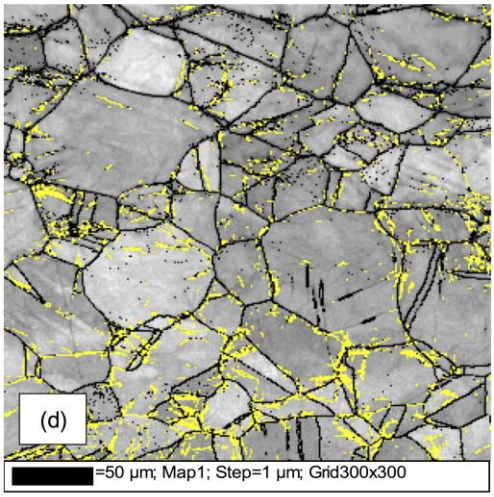

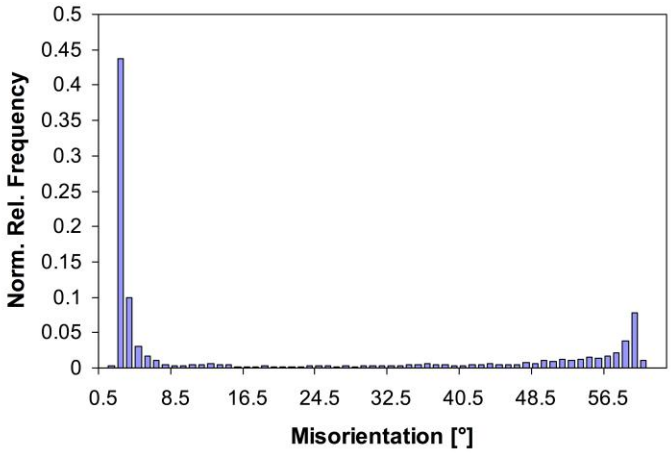

(11d)

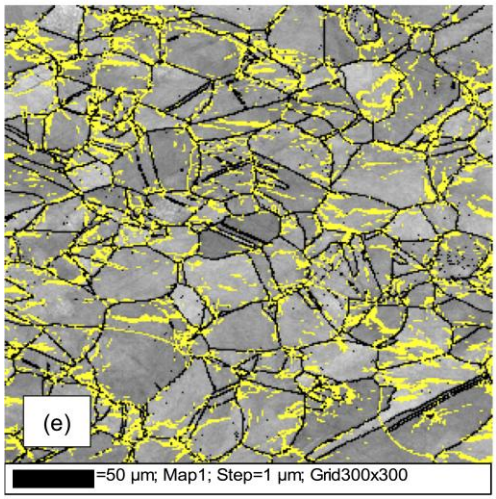

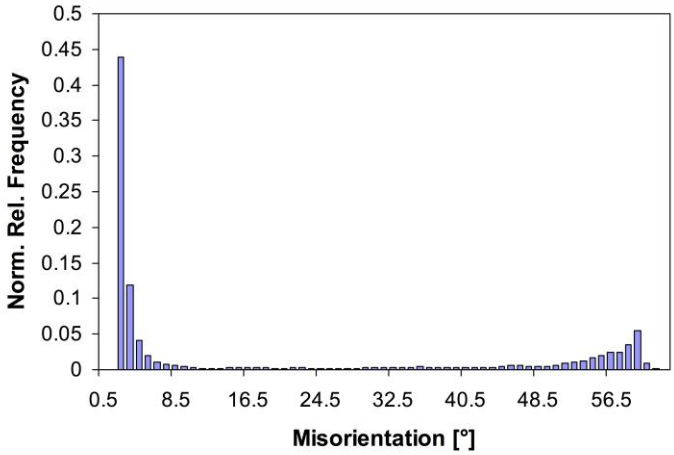

(11e)

Figure 11: Grain boundary mapping and misorientation distribution graph with increasing plastic deformation. High angle grain boundaries (HAGB) (>15°) are coloured in black and low angle grain boundaries (LAGB) (3-15°) are coloured in yellow. (LD: longitudinal direction of the tube, RD: radial direction)

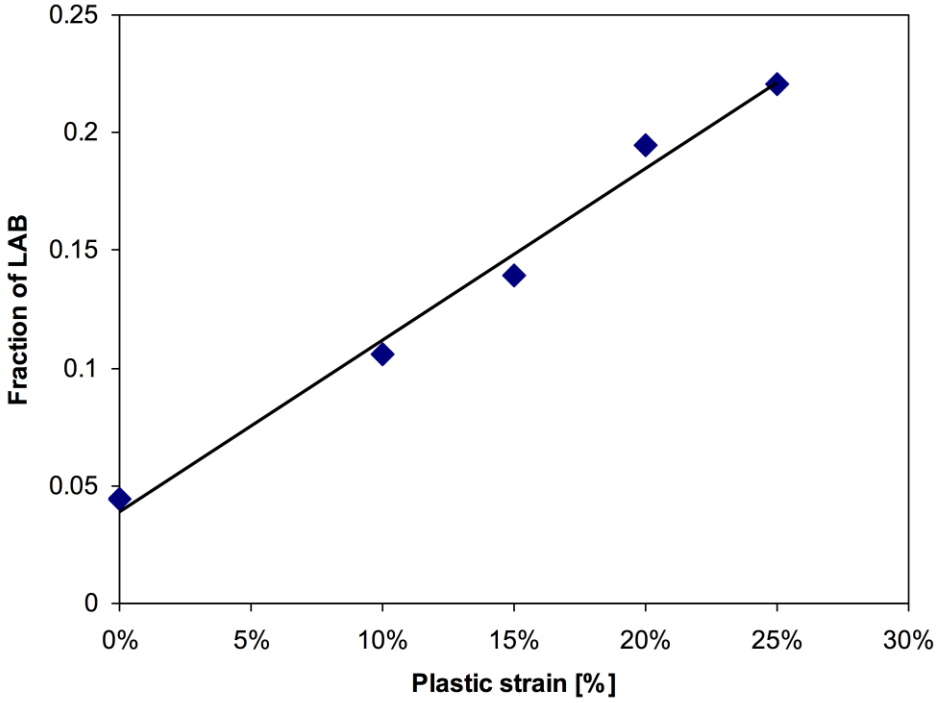

Figure 12 The fraction of LAB with increasing plastic deformation

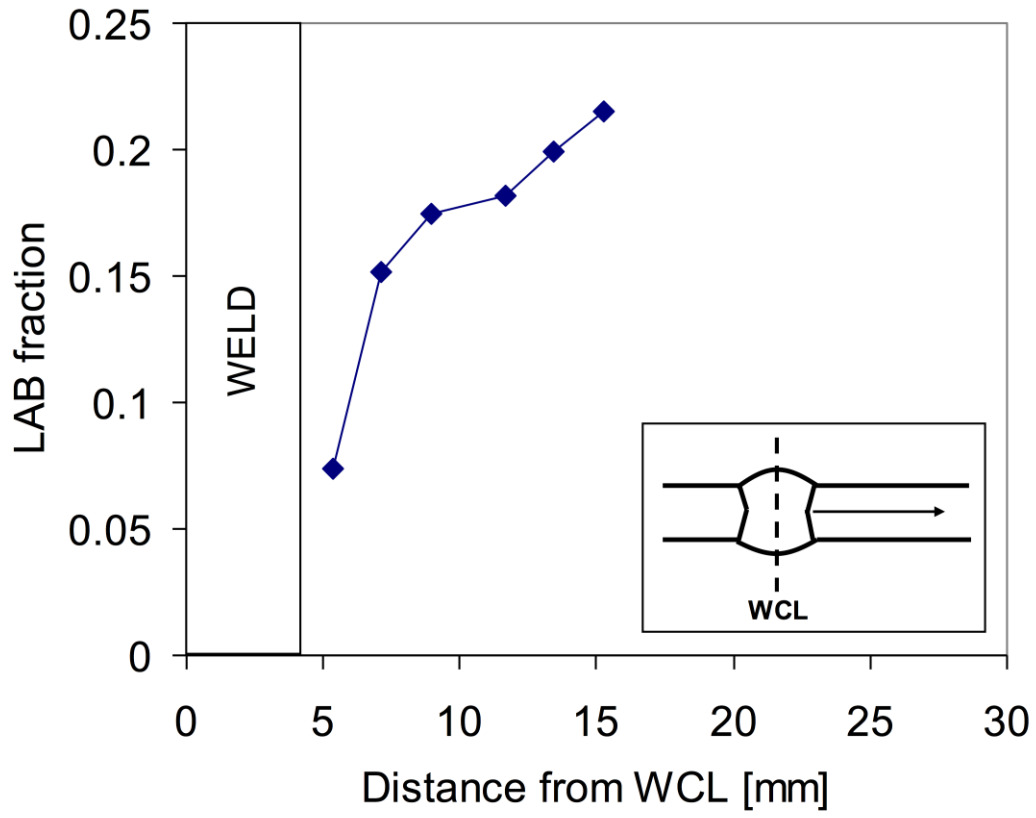

Figure 13 The variation of LAB fraction as a function of distance away from the WCL on LD-RD surface of 20% pre-strain sample. Each point represents an area of 300x900 μm2.

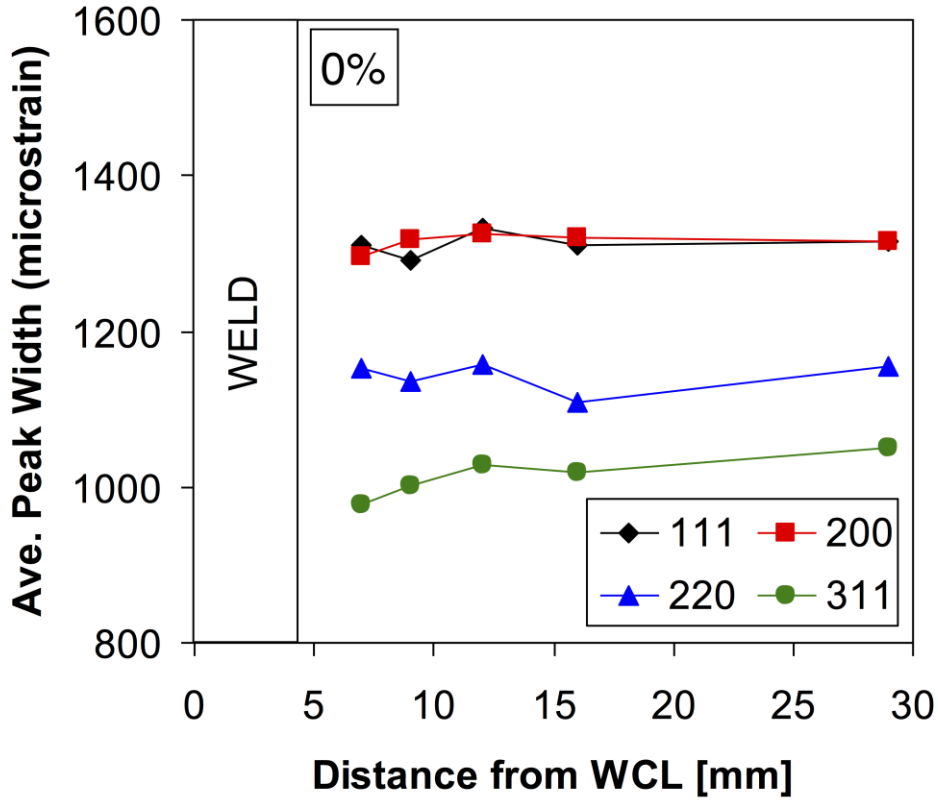

(a)

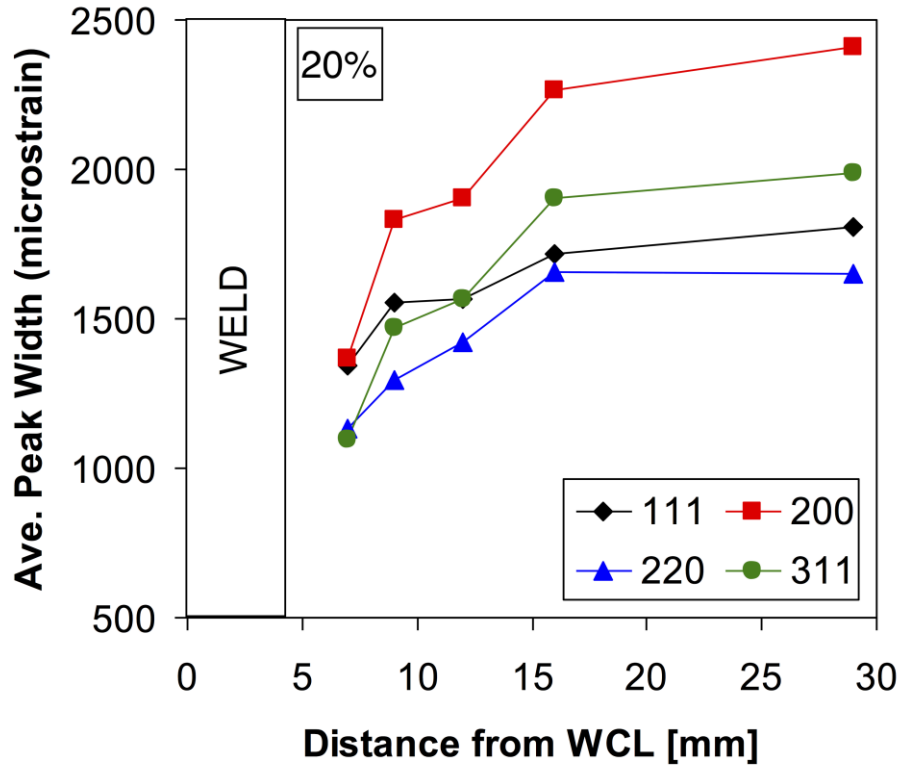

(b)

Figure 14 Variation of averaged peak width for hkl planes along the cross-weld specimens with (a) zero and (b) 20% pre-strain

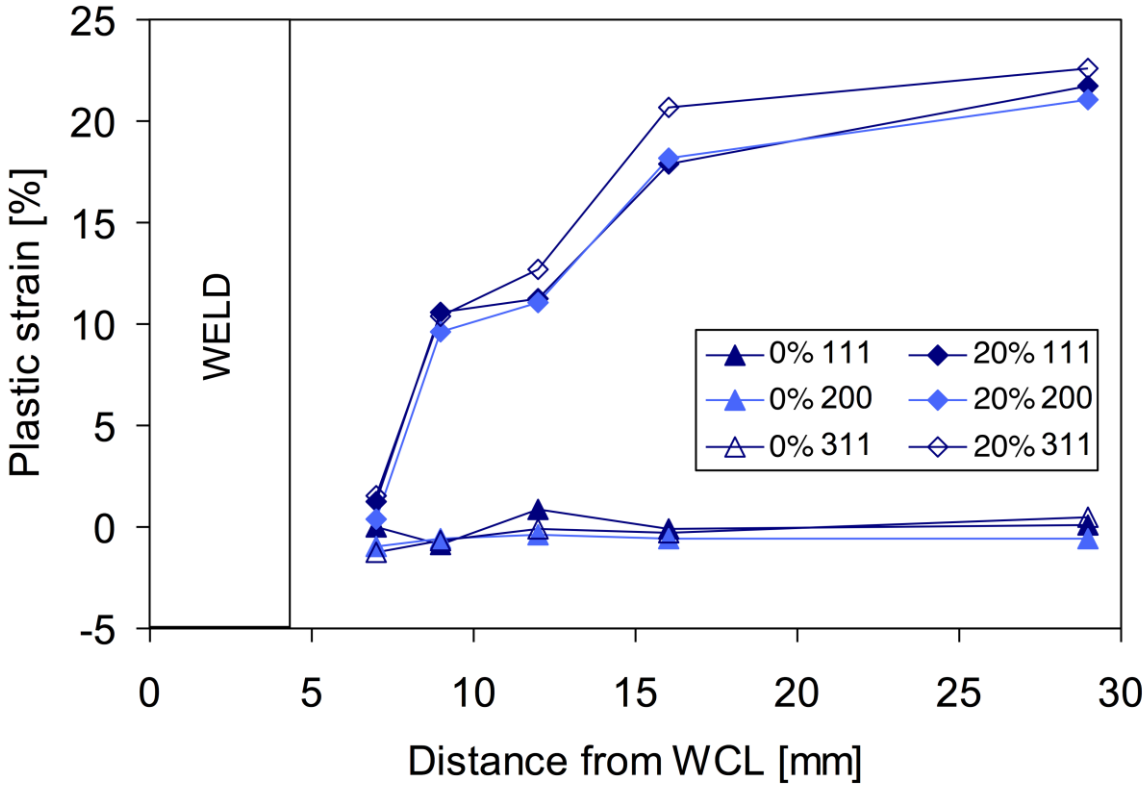

Figure 15 Prediction of plastic deformation on cross-weld specimens with zero and 20% pre-strain by calibrating the averaged peak widths obtained at different positions on these samples with averaged peak widths presented in Figure 2b

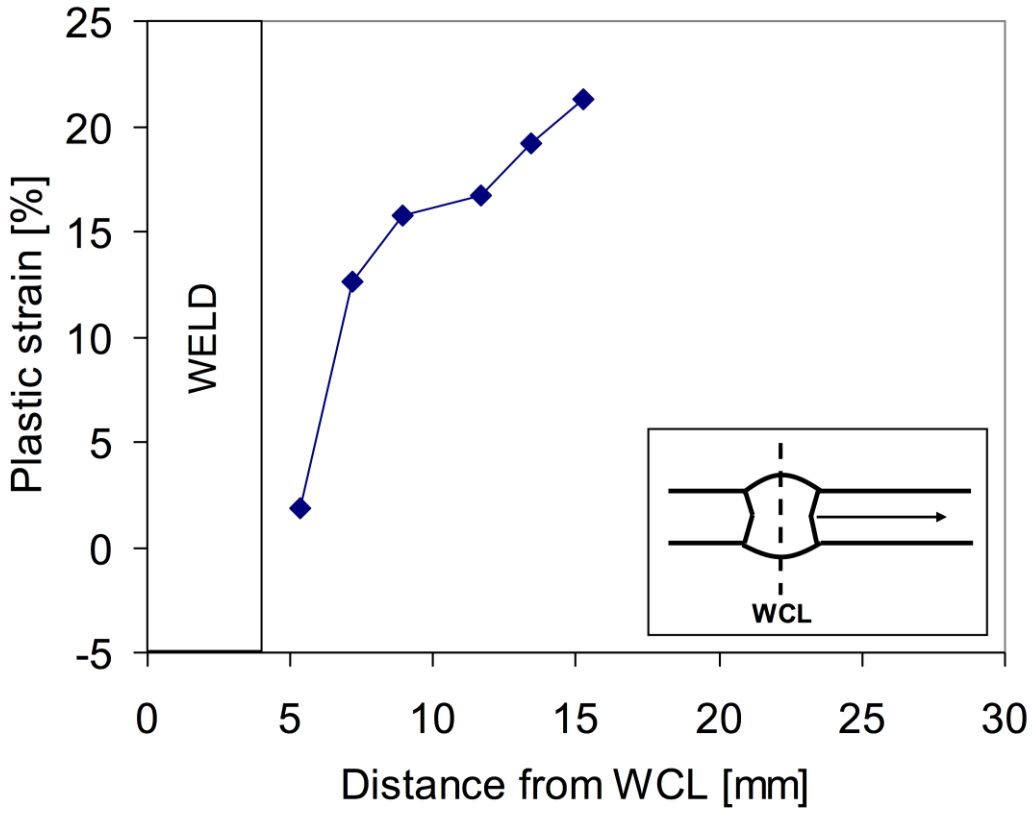

Figure 16 Prediction of plastic deformation on cross-weld specimen with 20% pre-strain by calibrating the LAB fraction at different positions on the same sample with LAB fraction presented in Figure 12.

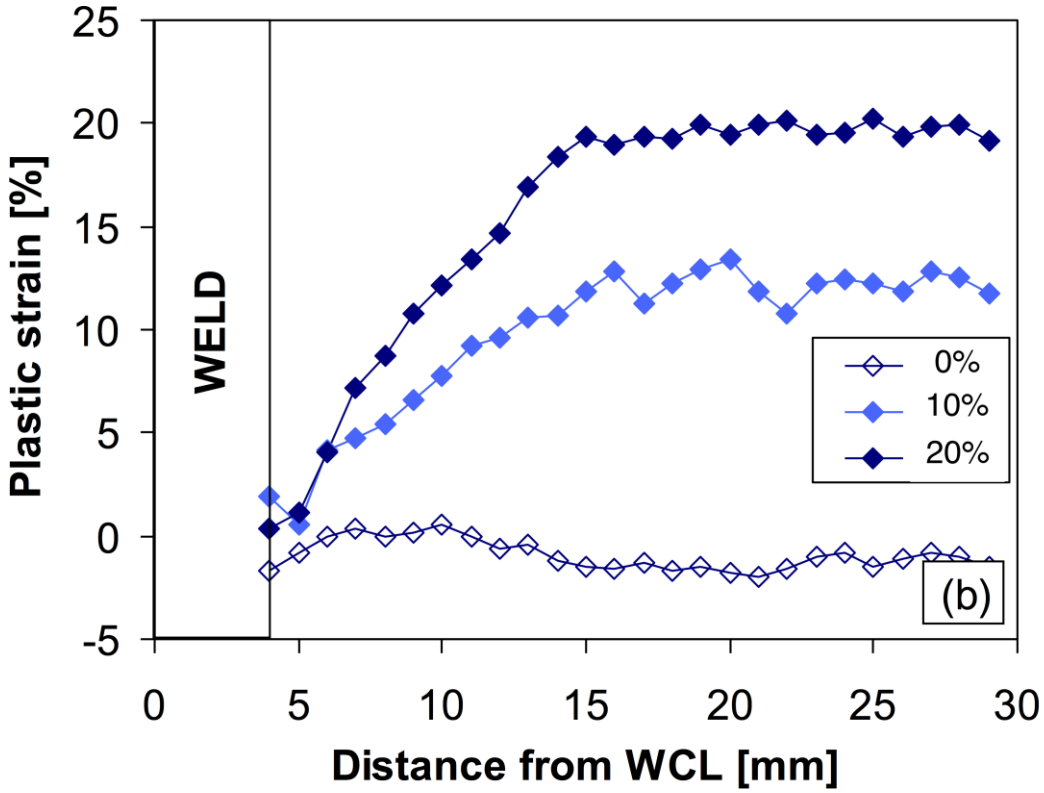

Figure 17 Prediction of plastic deformation on cross-weld specimen with zero, 10% and 20% pre-strain by calibrating the hardness measurements on these samples with the hardness variation with increasing plastic strain obtained from the parent samples.

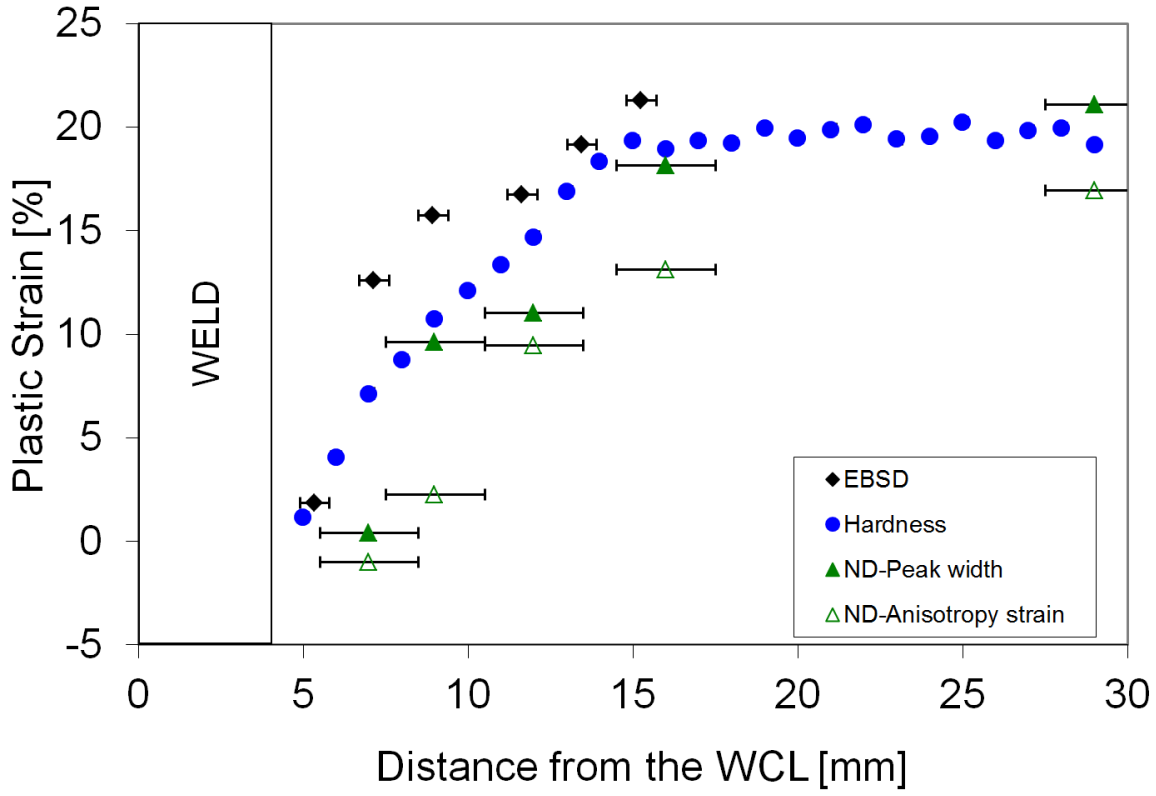

Figure 18 The comparison of plastic deformation predictions in the cross-weld sample with 20% pre-strain using EBSD, hardness, 111 peak width measurements and anisotropy strain (ND-anisotropy strain). Horizontal bars show the measurement volume for each data point.